Published in final edited form as:
Cell Mol Bioeng. 2012 December ; 5(4): 502–413.

Role of Epidermal Growth Factor-Triggered PI3K/Akt Signaling in the Migration of Medulloblastoma-Derived Cells

Veronica Dudu[1], **Richard A. Able Jr.**[1,2], **Veronica Rotari**[1], **Qingjun Kong**[3], and **Maribel Vazquez**[1]

[1]Department of Biomedical Engineering, The City College of the City University of New York (CCNY), 160 Convent Ave., Steinman Hall Room 403D, New York, NY 10031, USA

[2]Department of Biochemistry, The Graduate Center of the City University of New York, 365 Fifth Avenue, New York, NY 10016, USA

[3]The New York Center for Biomedical Engineering, The City College of the City University of New York (CCNY), 160 Convent Ave., Steinman Hall Room 401, New York, NY 10031, USA

Abstract

Medulloblastoma (MB) is the most common brain cancer diagnosed among children. The cellular pathways that regulate MB invasion in response to environmental cues remain incompletely understood. Herein, we examine the migratory response of human MB-derived Daoy cells to different concentration profiles of Epidermal Growth Factor (EGF) using a microfluidic system. Our findings provide the first quantitative evidence that EGF concentration gradients modulate the chemotaxis of MB-derived cells in a dose-dependent manner *via* the EGF receptor (EGF-R). Data illustrates that higher concentration gradients caused increased number of cells to migrate. In addition, our results show that EGF-induced receptor phosphorylation triggered the downstream activation of phosphoinositide-3 kinase (PI3K)/Akt pathway, while its downstream activation was inhibited by Tarceva (an EGF-R inhibitor), and Wortmannin (a PI3K inhibitor). The treatment with inhibitors also severely reduced the number of MB-derived cells that migrated towards increasing EGF concentration gradients. Our results provide evidence to bolster the development of anti-migratory therapies as viable strategies to impede EGF-stimulated MB dispersal.

Keywords

Chemotaxis; EGF; microfluidics; Daoy; PI3K/Akt

INTRODUCTION

Medulloblastoma (MB) is the most common malignant brain tumor in children, with a 60% survival rate 5 years after diagnosis.[9,31] The disease is difficult to treat *via* surgery because of high tumor invasiveness and tumor re-occurrence following resection and/or irradiation.[12] Despite the well-known metastatic potential of these pediatric tumors, the chemotactic migration of MB remains surprisingly understudied. The directed migration of brain tumor-derived cells is highly complex, involving interactions with extracellular matrix (ECM) and

Address correspondence to Maribel Vazquez, Department of Biomedical Engineering, The City College of the City University of New York (CCNY), 160 Convent Ave., Steinman Hall Room 403D, New York, NY 10031, USA. Electronic vazquez@ccny.cuny.edu.

ELECTRONIC SUPPLEMENTARY MATERIAL The online version of this article (doi:10.1007/s12195-012-0253-8) contains supplementary material, which is available to authorized users.

chemoattractants that either diffuse from blood vessels or are produced by neighboring cells.[6,24,33] The migration of cells derived from glioma, the most common malignant tumor in adult brain, has been extensively studied and shown to be highly dosage-dependent to signaling from three principal growth factors: Hepatocyte Growth Factor (HGF), Platelet-Derived Growth Factor (PDGF), and Epidermal Growth Factor (EGF).[3] By contrast, MB migration has been shown to depend on c-MET, the HGF receptor,[13] as well as the PDGF-receptor B (PDGFR-B), but EGF-R-dependent migration in MB has only recently been examined.

EGF-R, also known as ErbB1 or HER1, is a primary oncogene[19,34,40] whose over-expression is recognized as a significant step in the progression and pathology of brain tumors. Multiple mechanisms are involved in EGF-R activation, including expression of EGF and EGF-R by neighboring tumor or stromal cells, enhanced cell sensitivity for EGF-like ligands, and constitutively active EGF-R mutations that lead to ligand-independent activation of the receptor (reviewed in Hirata *et al.*[16]). The role of EGF-R in MB is highly significant, as the receptor is known to be expressed in the cerebellar granule neuron precursor cells (GNPCs)[35] whose dysregulation is suspected in MB tumorigenesis.[37] One quantitative study has illustrated that engineered over-expression of the EGF-R homolog, ErbB2, increased the migration of MB *in vitro*.[15] Another study has demonstrated that transactivation of EGF-R *via* PDGFR-B activity was able to guide MB migration *in vivo*.[2] Further, EGF-mediated migration has been shown to be concentration gradient-dependent, as breast cancer cells,[32] fibroblast cells[21] and glioma cells[1] responded to increasing gradients of EGF *via* higher motility *in vitro*.

In the present work, we utilize a microfluidic system[20] to examine the chemotactic migration of MB-derived cells towards EGF. We examine MB chemotactic dependency on EGF-R phosphorylation, consequent motility in response to a range of EGF concentration profiles, as well as activation of downstream phosphoinositide-3 kinase (PI3K)/Akt. Our results illustrate that EGF-initiated MB migration relies on the PI3K/Akt signaling pathway, and is ligand-dependent despite constitutive, basal EGF-R signaling. In addition, we demonstrate that larger concentration gradients of EGF stimulate increased numbers of MB cells to become motile. Our results comprehensively point to the significance of EGF-mediated invasion of MB, and highlight how targeting of the molecular triggers that drive MB migration may represent means to improve outcome, reduce relapse and impede metastasis.

MATERIALS AND METHODS

Cell Culture

The MB-derived Daoy cell line (#HTB-186, purchased from ATCC, Manassas, VA) was established from a tumor biopsy of a 4-year-old boy. Cells were cultured with sterile Eagle Minimum Essential Medium (EMEM) without phenol red (pH 7.1–7.4) (Mediatech Inc., Herndon, VA), supplemented with 2% L-glutamine (Mediatech Inc., Herndon, VA), 1% Penicillin–Streptomycin–Amphotericin B—100× solution (Mediatech Inc., Herndon, VA), and 10% fetal bovine serum (FBS) (Gemini Bio-Products, West Sacramento, CA). The cells were grown onto sterile polystyrene tissue culture flasks (BD Biosciences, Franklin Lakes, NJ) and incubated at 37 °C with 5% CO_2.

Antibodies and Immunocytochemistry

Immunocytochemistry was performed as described previously.[7] Briefly, Daoy cells grown on coverslips were fixed with paraformaldehyde (Sigma, St. Louis, MO) and labeled with mouse anti-phosphorylated-EGF-R (1:500) (Meridian Life Sciences, Saco, ME), mouse anti-

internal-EGF-R (1:500)—recognizing an internal epitope (Meridian Life Sciences, Saco, ME), rabbit anti-phosphorylated-Akt (1:200) (Cell Signaling, Danvers, MA), rabbit anti-phosphorylated-ERK-1/ERK-2 (1:200) (Cell Signaling, Danvers, MA), anti-mouse and anti-rabbit AlexaFluor® 488 or 594 antibodies (Invitrogen Molecular Probes, Eugene, OR). Transferrin AlexaFluor® 594 conjugate (Tf) and Cholera toxin subunit B AlexaFluor® 594 (CT-B) (both from Invitrogen Molecular Probes, Eugene, OR) were used to label the clathrin-mediated and clathrin-independent endocytic pathway, respectively. A 20 μg/mL solution of Tf or a 10 μg/mL solution of CT-B were applied and incubated with Daoy cells for 1 h at 37 °C. After antibody labeling, the cells were fixed with paraformaldehyde and mounted in glycerol. Each experiment was performed at least three times.

Stimulation and Inhibition of EGF-R and Akt

The stimulation of signaling pathways was adapted from the literature.[11] Briefly, monolayer cultures were separately incubated with 10, 100, and 1000 ng/mL EGF or EGF-Alexa 488 (Invitrogen Molecular Probes, Eugene, OR) for 20 min or 1 h at 37 °C. The active EGF-R was inhibited by incubating stimulated Daoy cells for 30 min or 1 h at 37 °C with 1 μM Tarceva,[17] kindly provided by Dr. Eric Holland, Memorial Sloan-Kettering Cancer Center, New York, NY). In a similar manner, the active PI3K was inhibited by incubating stimulated Daoy cells for 1 h at 37 °C with 0.5 μM Wortmannin (EMD-Calbiochem, Gibbstown, NJ). All cell samples were fixed and stained immediately following experimental protocols.

Confocal Microscopy and Image Analysis

Confocal laser scanning microscopy imaging was performed using a Leica TCS SP2 instrument with a 63× oil immersion objective (NA 1.4). Identical imaging conditions were used for each set of experiments. Analysis of the confocal images was performed using Matlab software (version 7.7.0.471). Fluorescence normalization was performed in order to measure whether the baseline of EGF-R, pEGF-R, pAkt, and pERK increased or decreased overall per cell. Basal gray levels were normalized per cell area and set to 1 in order to identify a control baseline per cell. A sample exceeding $n = 10$ was used for each experiment. Co-localization was determined using pixel area and defined as the 90–100% overlapping of data points. Co-localization with TF indicates markers coincide with clathrin-mediated endocytosis, while lack thereof with CT-B indicates no evidence for nonclathrin-medicated endocytosis. Statistical significance was analyzed by performing Anova t-tests with the InStat software (GraphPad Software Inc., La Jolla, CA).

Controlled Microenvironment

This study utilized our laboratory-developed μLane system, whose design and testing has been previously described.[20] The system was fabricated using contact photolithography, elastomeric molding of polydimethylsiloxane (PDMS), and ozone bonding of PDMS to glass microscope slides. The μLane relies on molecular diffusion to generate concentration gradients and sustain steady-state over a period of 2–3 days. The system consists of a single, closed microchannel that connects two fluidic reservoirs, called the sink and the source chambers, as shown in Figs. 1a and 1b. The microchannel used in this study is 7000 μm in length and 95 μm in hydraulic diameter, while the source and sink chambers contain a 9 and 170 μL volume, respectively.

Molecular transport within ECM of the μLane was validated experimentally and computationally using Dextran (6 kDa; Invitrogen, Eugene, OR) as a model, based on similar hydrodynamic, or Stokes radii, and molecular configurations to EGF.[4,28] Experimental measurement of Dextran diffusion was performed as described in the literature,[18] by tracking the displacement of the fluorescently-labeled molecule. In order to

determine the concentration distribution within our system, 40 μg/mL Dextran was mixed with 2.5 mg/mL Growth Factor-Reduced Matrigel (BD Biosciences, San Jose, CA), used as ECM, and loaded into the microchannel. The source and sink chambers were subsequently filled with EMEM. Fluorescent Dextran diffusion within the microchannel was imaged at different positions along the channel using time-lapse microscopy using the Nikon TE2000 inverted microscope with a 20× long working distance dry objective (NA 0.40/WD 3.0 mm) and a cooled CCD camera (CoolSNAP EZ, Photometrics, Tucson, AZ). Images were recorded every hour for 84 h using Nikon software (Nikon Instrument Element 2.30 with 6D module, Morrell Instrument Company Inc., Melville, NY). The fluorescence intensity was measured at all time-points using the Nikon software. Experimental measurement of Dextran transport illustrated a transient evolution of a linear, steady-state concentration gradient along the microchannel after t = 70 h, as shown in Fig. 1c.

Computational modeling of Dextran concentration profiles within the μLane system was performed using Finite Element Modeling (FEMLab version 3.2, Comsol Inc. Burlington, MA to model the one-dimensional diffusion equation:

$$\left[\frac{\partial C}{\partial t} = D\frac{\partial^2 C}{\partial x^2}\right] \quad (1)$$

where C (mg/mL) is the concentration, and D (m^2/s) is diffusivity.[21] FEM computation used an initial reagent concentration in the source chamber and microchannel of 40 μg/mL in order to match the experimental conditions, and an initial concentration in the sink chamber of 0 μg/mL. Reported diffusivity values of Dextran[10,23,30,38] were substituted into the model in order to generate spatial concentration profiles within the microchannel that most accurately modeled those measured experimentally. Computational predictions illustrated in a linear, steady-state gradient along the 7-mm-long microchannel after t = 70 h (Fig. 1d). Finite Element Modeling of the Dextran concentration profiles generated within the microchannel and in the source and sink chambers, respectively, is shown in Fig. 1e. We employed the same modeling to predict that EGF diffusion will achieve steady-state within t = 70 h within the μLane design used in this study (Figs. 1c and 1d).

Cell Migration Experiments

EGF at different concentrations (10, 100, or 1000 ng/mL and 0 ng/mL for control) was mixed with 2.5 mg/mL Growth Factor-Reduced Matrigel and loaded into the microchannel and the source chamber *via* syringe. The μLane systems were placed in a micro-incubator (Warner Instruments LLC, Hamden, CT) that was maintained at 37 °C and mounted on a motorized stage of a Nikon TE2000 inverted microscope. No CO_2 control was used in this study. However, the pH-indicator medium used for each test did not indicate significant changes in pH. MB cells at a cell density of 10^6/mL and in a solution of EMEM were added into the sink reservoir. Cells were loaded such that they adhered evenly to the bottom of the chamber and along its microchannel interface. Cell movement into the microchannel from the sink chamber was monitored through light microscopy, using a 20× long working distance dry objective and a cooled CCD camera. Experiments using long working distance objectives verified that cells were migrating within the entire 3D ECM during testing, but data captured *via* inverted scope can only measure those cells closest to the coverslip. Images of cells moving from the sink chamber into the microchannel were recorded for 72 h using Nikon software (Nikon Instrument Element 2.30 with 6D module, Morrell Instrument Company Inc., Melville, NY). The total number of migrating cells into the microchannels were counted, and the total distance migrated by each of those cells was measured using Nikon software. Note that experiments utilized serum in order to better match the conventional Boyden chamber assays used by previous work from our lab[1,21] and others[3]

that utilize the assays as benchmarks for migration. As demonstrated previously in the literature,[41] Boyden chamber experiments using serum-starved MB cells vs. non-serum starved cells confirmed near identical chemotactic behaviors (data in Supplemental Fig. 1).

Migration experiments were performed using known inhibitors of EGF and PI3K pathways. Cells were separately treated for 1 h with 1 μM Tarceva (EGF-R inhibitor), or with 0.5 μM Wortmannin (PI3K inhibitor). Treated cells were loaded into the sink chamber of the μLane and their migration imaged and analyzed as described before. Note that inhibitor experiments were only performed using the gradients generated under experimental conditions of 1000 ng/mL EGF. For all migration experiments, the data was plotted and statistical significance was analyzed *via* Anova tests with InStat software (GraphPad Software Inc., La Jolla, CA).

Lastly, recorded data for chemotactic migration was distinguished from chemokinetic movement (i.e., non-directional) by relying on controls that filled the entire microsystem (reservoirs and channel) with ECM to reveal minimal cell movement in the absence of exogenous EGF. Further, changes in cell chemokinesis in the presence of different EGF concentrations (10, 100, and 1000 ng/mL) were statistically insignificant from that of control experiments as observed *via* measuring positional changes of cell centroids ($n > 15$) during a 40-h test period.

Cell Cytoplasmic Extensions and Cell Shape Index

Cells were cultured within 2.5 mg/mL of Matrigel with or without 100 ng/mL EGF for up to 100 h. Images of the cells were recorded using the Nikon TE2000 and Nikon software. The cytoplasmic extensions of cells were counted and their numbers were averaged at the focal plane illustrating the maximum cell area. The average cell morphology was analyzed using the cell shape index (CSI),[36] as done previously by our group[20]:

$$\left[\mathrm{CSI}=\frac{4\pi A}{P^2}\right] \quad (2)$$

where A represents the cell projected area, and P denotes the cell perimeter. Statistical significance of data differences was analyzed *via* Student t-tests using InStat software.

RESULTS

Basal and Ligand-Activated EGF-R in MB

In order to examine EGF-induced migration of MB, we first investigated EGF-R activation, inhibition, and localization. The total EGF-R population within the MB cells studied was detected *via* an antibody that recognized the intracellular region of the receptor, iEGF-R. Here, iEGF-R was labeled in non-stimulated cells (Fig. 2a), in cells stimulated with EGF (Fig. 2b), and in cells where the effect of the stimulation was inhibited by using Tarceva (Fig. 2c). Tarceva is a commercial compound known to inhibit EGF-R autophosphorylation without affecting EGF-R expression or surface receptor density.[14] No significant difference in total intensity levels of EGF-R between stimulated and Tarceva-inhibited cells were measured with respect to controls (Fig. 2d). Next, immunolabeling was performed with an antibody that recognized phosphorylated EGF-R (pEGF-R). Results illustrated that MB-derived cells exhibited basal levels of activated EGF-R (Fig. 2e). Interestingly, EGF stimulation of MB increased cellular levels of pEGF-R (Fig. 2f) by 2.8 fold (Fig. 2h), indicative of a ligand-dependent EGF-R response regardless of basal EGF-R signaling. Treatment with Tarceva consistently abolished ligand-induced EGF-R phosphorylation (Fig. 2g), as levels of phosphorylated EGF-R were similar to those detected in non-stimulated cells (Fig. 2h). Next, MB-derived cells were incubated with Transferrin (Tf), a marker of the

clathrin-mediated endocytic pathway and Cholera Toxin Subunit-B (CT-B), a marker of the clathrin-independent endocytic pathway, as done previously by our group.[8] In MB-derived cells, iEGF-R was seen to co-localize predominantly with Tf: 92 ± 3% (Figs. 2i1–3 and 2j), but only 14 ± 4% with CT-B (Fig. 2j). We note that co-localization with TF indicates markers coincide with clathrin-mediated endocytosis, while lack thereof with CT-B indicates no evidence for non-clathrin-medicated endocytosis.[25]

EGF Induces Akt Phosphorylation in MB

The next set of experiments examined the role of PI3K/Akt and MAPK/ERK signaling in the EGF-R-induced response of MB, as activation and cross-talk of these pathways downstream of activated EGF-R is well-known in glioblastoma and breast cancer migration.[22,43] Levels of phosphorylated Akt (pAkt) in cells stimulated with EGF (Fig. 3b) were seen to increase 3.32-fold with respect to those in non-stimulated cells (Figs. 3a and 3i). Consistently, pAkt levels were drastically reduced to control levels when EGF signaling was inhibited by Tarceva (Figs. 3c and 3i), as well as when PI3K signaling was inhibited by Wortmannin (Figs. 3d and 3i). Levels of phosphorylated ERK-1/2 (pERK) in cells stimulated with EGF (Fig. 3f) increased 1.81-fold with respect to non-stimulated cells (Figs. 3e and 3j), and were similar to levels for which EGF signaling was inhibited by Tarceva (Figs. 3g and 3j). In cells treated with Wortmannin, pERK levels were similar to those measured in the absence of the PI3K inhibitor (Figs. 3h and 3j), indicating negligible cross-talk between MAPK/ERK and PI3K/Akt pathways.

MB Morphology and Proliferation Within μLane System

The μLane system was next used to examine the EGF-stimulated behavior of MB-derived cells within ECM. MB cultured within ECM-alone and ECM supplemented with 10, 100, and 1000 ng/mL EGF were seen to grow, divide, and survive inside of the microchannel for 100 h. Cellular changes were measured *via* the CSI, number of cytoplasmic extensions per cell, and observed proliferation time within the microsystem. Cells within ECM-alone exhibited rounder morphology (Fig. 4a), while cells in ECM exposed to EGF exhibited elongated morphology (Fig. 4b). The average, measured CSI was lower for cells exposed to EGF (Fig. 4c), consistent with CSI definition, which approaches 1 for an amoeboidal cell and decreases towards zero for an elongated or branched cell (Eq. 2). We note that the CSI of MB cells remained statistically insignificant when treated with EGF-R inhibitors. Similarly, the average number of cellular extensions was not statistically different between stimulated and non-stimulated cells (Fig. 4d). Lastly, MB cell division was seen to occur consistently between 42 and 46 h in all microchannel experiments. As a result, analysis of cell behavior prior to $t = 40$ h was deemed to be primarily migratory and non-proliferative, while MB behavior post $t = 40$ h was considered both migratory and proliferative in all subsequent analyses.

EGF Concentration Profiles Generated Within μLane System

EGF transport within the μLane generated a range of concentrations and gradients along the microchannel length over time. The concentration gradients present along the μLane from $t = 0$ h to $t = 72$ h were calculated by measuring the change in EGF concentration over a fixed microchannel distance. Mathematically, gradients can be represented by the changing slope of the curves. Note that because EGF is distributed non-linearly along the microchannel length prior to steady-state (as shown in Fig. 1c), concentration gradients are also highly non-linear during this time, and encompass several orders of magnitude per experimental condition. Steady-state EGF distributions along the microchannel generated by using separate solutions of 10, 100, and 1000 ng/mL concentrations in the source chamber each exhibited linear steady-state concentration gradients at $t = 70$ h.

EGF-Mediated Chemotaxis of MB Within μLane System

The migration of MB-derived cells was then measured in response to the separate EGF concentration profiles described above. Microenvironments generated by using 1000 ng/mL in the sink chamber attracted the largest numbers of cells to migrate into the microchannel, both prior to and after MB proliferation (i.e., before and after $t = 40$ h, respectively). As shown in Fig. 5a, the numbers of cells that migrated out of the sink chamber and into the microchannel prior to 40 h (non-proliferative) increased when exposed to increasing EGF concentrations and gradients. Numbers of cells observed within microchannels between $t = 42$ h and $t = 72$ h (motile and proliferative) similarly increased with EGF concentration and gradient, although in larger proportions than in experiments measuring migration alone. Large numbers of cells were drawn into the channel when exposed to concentration gradients generated by using 10, 100, and 1000 ng/mL concentrations. In addition, the migration of MB treated with the inhibitors Tarceva and Wortmannin was examined within the μLane environment generated using 1000 ng/mL EGF. As seen, the numbers of cells that responded to EGF when EGF-R signaling was inhibited by Tarceva, and when the PI3K pathway was inhibited by Wortmannin, were less than 5% of the controls in each case (Fig. 5a).

Additionally, the average cell distances traveled within the different environments of the μLane were calculated for pre-proliferative cells ($t < 40$ h) and for cells undergoing both migration and proliferation ($t = 40$ h and $t = 72$ h). As seen in Fig. 5b, the average cell distances traveled prior to $t = 40$ h (i.e., migration only) and between $t = 40$ h and $t = 72$ h (migration and proliferation) were lowest for controls, and increased slightly with EGF concentration and gradient. However, no statistical difference was measured between the different EGF concentrations.

Lastly, the average EGF concentration and concentration gradient experienced by MB cells that became motile over the experimental time was calculated using the mathematically-derived EGF distribution within the μLane system described in Fig. 1. As mathematically predicted by Fick's Law, both the absolute gradient and absolute EGF concentration present in the channel changed with time depending upon the initial EGF condition used (i.e., 10, 100, and 1000 ng/mL).

During all experiments, MB cells were observed to become motile at early time points, within microenvironments where cells were exposed to the highest EGF gradients and highest EGF concentrations. Cells then appeared to become non-motile at later times, when exposed to microenvironments with low EGF concentration and low EGF gradient. For all experiments, changes in cell displacement within the channel were observed to approach zero when exposed to EGF concentrations that were below ~0.85 of the initial EGF concentration used. Similarly, in all experiments, cells became immobile when experiencing an average decrease in relative concentration gradient of one order of magnitude between the experimentally-measured time of $t = 1$ h, and the final pre-proliferation time of $t = 40$ h.

The average concentration experienced by motile cells between $t = 1$ h and $t = 40$ h within our experiments that used initial 10 ng/mL concentration of EGF to generate EGF gradients within the microchannel was ~9.0 ng/mL. Similarly, the average concentration experienced by cells that became motile when exposed to concentration gradients generated by initial EGF concentrations of 100 ng/mL was ~90 ng/mL. Lastly, cells exposed to concentration gradients within the microchannel generated by initially using 1000 ng/ml of EGF experienced an average concentration of ~900 ng/mL. In addition, motile cells experienced a great range of concentration gradients during the transient evolution of the EGF profile within the microchannel. Cells that became motile when exposed to concentration gradients generated by using EGF of 10 ng/mL experienced an average concentration gradient of ~1

ng/mL per mm of microchannel. Similarly, motile cells exposed to EGF profiles created using 100 ng/L of EGF experienced an average concentration gradient of ~10 ng/mL per mm of microchannel, while motile cells within EGF profiles generated using 1000 ng/mL in our experiments experienced an average concentration gradient of ~100 ng/mL per mm.

DISCUSSION

The migration of cells from pediatric brain tumors has been largely understudied despite their high tumor metastatic potential and aggressive invasion into healthy brain. While EGF-R is known to play significant roles in the chemotaxis of tumor cells within adult brain, the EGF-induced migration of MB has only recently been examined. The current study examined the activation of EGF-R-mediated pathways in MB and directly correlated MB migratory response to a range of EGF concentrations and gradients generated by using a microfluidic system.

Initial immunocytochemistry experiments demonstrated constitutively-active EGF-R signaling in the MB cells studied. Interestingly, EGF-R response was also ligand-dependent, as increased EGF-R phosphorylation and co-localization with endosomes was observed upon EGF stimulation. These results confirm the findings of other studies,[26] which documented basal EGF-R expression in Daoy cells *via* quantitative PCR, as well as confirmed Daoy autocrine expression of EGF and TGF-α ligands. These data illustrate that EGF-R signaling is appreciable for MB cells even in the presence of exogenous growth factors. The finding that EGF-R in MB can respond to external EGF despite basal EGF-R signaling bolsters the hypothesis that exogenous EGF stimulation is able to stimulate chemotactic responses in MB-derived cells. When examining EGF activation of the PI3K and MAPK pathways, our data illustrated that the PI3K pathway was activated by EGF and inactivated when EGF signaling was inhibited by Tarceva, a kinase inhibitor, and Wortmannin, an Akt inhibitor. However, our data illustrated minimal effect of either compound on pERK, suggesting MAPK is only minimally involved in the EGF-R-induced chemotactic signaling of these cells. This result is in conflict with existing research, which illustrated decreased pERK activation in response to the kinase inhibitor, gefitinib, in both serum starved and serum treated Daoy cells.[5,29] However, we note that the lack of inhibited pERK seen in our study could be due to a weaker sensitivity to Tarceva vs. gefitinib in Daoy cells, as the gefitinib kinase inhibitor specifically targets ErbB2, which is known to be less expressed in Daoy than other MB cell lines.[26]

We next examined EGF-mediated migration of MB in a microfluidic system, which enables precise control of the cellular microenvironment, as well as real-time cell visualization and measurement of cell behavior. While conventional systems such as transwell assays provide quantitative data to describe numbers of cells that become motile in response to a stimulus, the application of microdevices enables experiments to examine mechanistic parameters such as motility, polarization, directionality or the sensitivities of individual cells to concentration gradients and thresholds. However, we reiterate here that because our experiments were conducted continuously for over 72 h, measurements of traveled cell distances include effects from all transient, non-linear gradients generated during the temporal evolution of each steady-state gradient examined (as shown in Figs. 1c and 1d). As a result, the data includes transient effects of higher concentrations and higher gradients present prior to steady-state at $t = 70$ h.

A first technical point of interest in this work is that Matrigel provided a suitable ECM for which to evaluate MB chemotactic migration. This is of interest because the diversity of motility modes utilized by cancer cells[39] has called into question the use of Matrigel given the matrix's constituent, biologically-relevant molecules (reviewed in Yuan *et al.*[42]). Our

data illustrate that the Matrigel effects were consistent with each experiment and every EGF concentration used, and thus did not contribute to the differences in migratory measurements recorded. In controls, a small, but measurable, number of cells were observed to migrate into the microchannel as a likely result of MB chemokinesis. But the number of cells that responded in our system as a result of experimental conditions greatly outweighed the presumably-constant, baseline number of cells that migrated into the system as a result of the Matrigel alone.

Migration experiments in our microdevice revealed that the numbers of motile cells increased with increasing EGF concentration, both before and after proliferation occurred within microchannels. Results of other studies from our lab, as well as from others, have shown behaviors of cell populations that migrate preferentially in low concentration gradient fields and high concentration,[1] or high concentration gradient fields and low concentration.[21,27] Our current work illustrates that MB cells migrate preferentially in high concentration gradient fields accompanied by high concentration. Interestingly, the distance traveled within the microchannels was not statistically significant between the experiments that utilized exogenous EGF, although the average cell distance traveled when exposed to any examined amount of EGF was statistically higher than that of the control. Here, we observed that lower concentration gradient fields correlated with lower motilities: As cells migrated in the microchannel they experienced diminishing concentration gradients until cell motility approached zero. We posit that MB migrated in larger numbers into the channel when stimulated by increased concentration because a higher concentration threshold is needed to overcome the constitutively active EGF signaling in MB. Further, since the distance traveled by these cells was statistically insignificant, we propose that higher EGF concentration works to stimulate a higher fraction of motile cells to invade the channel, but that it is the change in relative concentration gradient that then determines the migration rate.

These results are significant because similar *in vitro* experiments have illustrated that gradient chemosensitivity is cell type dependent. Our data becomes among the first to illustrate that the motility of MB-derived cells increases in larger concentration gradient fields, not only in response to higher EGF concentration.

CONCLUSION

The current report demonstrates the role of EGF-induced Akt activation in the migration of MB-derived cells *in vitro*. Results of microfluidic-based experiments correlated MB increased chemotactic response with gradient fields, providing impetus for the development of new anti-migratory strategies as therapeutic agents.

Supplementary Material

Refer to Web version on PubMed Central for supplementary material.

Acknowledgments

This work has been supported by The National Institutes of Health (R21 CA 118255 and U54 MICHOR), The Pediatric Brain Tumor Foundation, and PSC-CUNY (No. 69424). The authors wish to thank Ms. Jennifer Rico for her technical assistance in this work.

REFERENCES

1. Able RA, Ngnabeuye C, Beck C, Holland EC, Vazquez M. Low concentration microenvironments enhance the migration of neonatal cells of glial lineage. Cell. Mol. Bioeng. 2012; 5(2):128–142.

2. Abouantoun TJ, Macdonald TJ. Imatinib blocks migration and invasion of medulloblastoma cells by concurrently inhibiting activation of platelet-derived growth factor receptor and transactivation of epidermal growth factor receptor. Mol. Cancer Ther. 2009; 8(5):1137–1147. [PubMed: 19417143]
3. Brockmann MA, Ulbricht U, Gruner K, Fillbrandt R, Westphal M, Lamszus K. Glioblastoma and cerebral microvascular endothelial cell migration in response to tumor-associated growth factors. Neurosurgery. 2003; 52(6):1391–1399. [PubMed: 12762884]
4. Cadena DL, Chan CL, Gill GN. The intracellular tyrosine kinase domain of the epidermal growth factor receptor undergoes a conformational change upon autophosphorylation. J. Biol. Chem. 1994; 269(1):260–265. [PubMed: 8276804]
5. Calabrese C, Frank A, Maclean K, Gilbertson R. Medulloblastoma sensitivity to 17-allylamino-17-demethoxygeldanamycin requires MEK/ERKM. J. Biol. Chem. 2003; 278:24951–24959. [PubMed: 12709419]
6. Condeelis J, Segall JE. Intravital imaging of cell movement in tumours. Nat. Rev. Cancer. 2003; 3(12):921–930. [PubMed: 14737122]
7. Dudu V, Ramcharan M, Gilchrist ML, Holland EC, Vazquez M. Liposome delivery of quantum dots to the cytosol of live cells. J. Nanosci. Nanotechnol. 2008; 8(5):2293–2300. [PubMed: 18572640]
8. Dudu V, Rotari V, Vazquez M. Sendai virus-based liposomes enable targeted cytosolic delivery of nanoparticles in brain tumor-derived cells. J. Nanobiotechnol. 2012; 10(1):9.
9. Duffner PK, Horowitz ME, Krischer JP, Burger PC, Cohen ME, Sanford RA, Friedman HS, Kun LE. The treatment of malignant brain tumors in infants and very young children: an update of the Pediatric Oncology Group experience. Neuro. Oncol. 1999; 1(2):152–161. [PubMed: 11554387]
10. Ekani-Nkodo A, Fygenson DK. Size exclusion and diffusion of fluoresceinated probes within collagen fibrils. Phys. Rev. E. 2003; 67(2 Pt 1):021909.
11. Fukazawa T, Miyake S, Band V, Band H. Tyrosine phosphorylation of Cbl upon epidermal growth factor (EGF) stimulation and its association with EGF receptor and downstream signaling proteins. J. Biol. Chem. 1996; 271(24):14554–14559. [PubMed: 8662998]
12. Girish M, Nair S, Muthurethinam T, Krishnakumar K, Bhattacharya RN. Medulloblastoma in children: prognostic factors and predictors of outcome. J. Pediatr. Neurosci. 2006; 1(1):16–20.
13. Guessous F, Zhang Y, diPierro C, Marcinkiewicz L, Sarkaria J, Schiff D, Buchanan S, Abounader R. An orally bioavailable c-Met kinase inhibitor potently inhibits brain tumor malignancy and growth. Anticancer Agents Med. Chem. 2010; 10(1):28–35. [PubMed: 20015006]
14. Herbst R, Erlotinib S. Clin. Adv. Hematol. Oncol. 2005; 3(2):124–141.
15. Hernan R, Fasheh R, Calabrese C, Frank AJ, Maclean KH, Allard D, Barraclough R, Gilbertson RJ. ERBB2 up-regulates S100A4 and several other prometa-static genes in medulloblastoma. Cancer Res. 2003; 63(1):140–148. [PubMed: 12517790]
16. Hirata A, Ogawa S, Kometani T, Kuwano T, Naito S, Kuwano M, Ono M. ZD1839 (Iressa) induces anti-angiogenic effects through inhibition of epidermal growth factor receptor tyrosine kinase. Cancer Res. 2002; 62(9):2554–2560. [PubMed: 11980649]
17. Huse JT, Holland EC. Targeting brain cancer: advances in the molecular pathology of malignant glioma and medulloblastoma. Nat. Rev. Cancer. 2010; 10(5):319–331. [PubMed: 20414201]
18. Kim MJ, Breuer KS. Enhanced diffusion due to motile bacteria. Phys. Fluids. 2004; 16(9):L78–L81.
19. Kim H, Muller WJ. The role of the epidermal growth factor receptor family in mammary tumorigenesis and metastasis. Exp. Cell Res. 1999; 253(1):78–87. [PubMed: 10579913]
20. Kong Q, Able R, Dudu V, Vazquez M. A micro-fluidic device to establish concentration gradients using reagent density differences. J. Biomech. Eng. 2010; 132(12):121012. [PubMed: 21142326]
21. Kong Q, Majeska RJ, Vazquez M. Migration of connective tissue-derived cells is mediated by ultra-low concentration gradient fields of EGF. Exp. Cell Res. 2011; 317:1491–1502. [PubMed: 21536028]
22. Kruger JS, Reddy KB. Distinct mechanisms mediate the initial and sustained phases of cell migration in epidermal growth factor receptor-overexpressing cells. Mol. Cancer Res. 2003; 1(11): 801–809. [PubMed: 14517342]
23. Lang I, Scholz M, Peters R. Molecular mobility and nucleocytoplasmic flux in hepatoma cells. J. Cell Biol. 1986; 102(4):1183–1190. [PubMed: 2420804]

24. Lauffenburger DA, Horwitz AF. Cell migration: a physically integrated molecular process. Cell. 1996; 84(3):359–369. [PubMed: 8608589]
25. Le Roy C, Wrana JL. Clathrin- and non-clathrin-mediated endocytic regulation of cell signalling. Nat. Rev. Mol. Cell Biol. 2005; 6(2):112–126. [PubMed: 15687999]
26. Meco D, Servidei T, Riccardi A, Ferlini C, Cusano G, Zannoni GF, Giangaspero F, Riccardi R. Antitumor effect in medulloblastoma cells by gefitinib: ectopic HER2 overexpression enhances gefitinib effects in vivo. Neuro. Oncol. 2009; 11:250–259. [PubMed: 19033425]
27. Mosadegh B, Saadi W, Wang SJ, Jeon NL. Epidermal growth factor promotes breast cancer cell chemotaxis in CXCL12 gradients. Biotechnol. Bioeng. 2008; 100(6):1205–1213. [PubMed: 18553401]
28. Nicholson C, Tao L. Hindered diffusion of high molecular weight compounds in brain extracellular micro-environment measured with integrative optical imaging. Biophys. J. 1993; 65(6):2277–2290. [PubMed: 7508761]
29. Ono M, Kuwano M. Molecular mechanisms of epidermal growth factor receptor (EGFR) activation and response to gefitinib and other EGFR-targeting drugs. Clin. Cancer Res. 2006; 12(24):7242–7251. [PubMed: 17189395]
30. Payet L, Ponton A, Lger L, Hervet H, Grossiord JL, Agnely F. Self-diffusion in chitosan networks: from a gel–gel method to fluorescence recovery after photoble-aching by fringe pattern. Macromolecules. 2008; 41(23):9376–9381.
31. Reddy AT. Advances in biology and treatment of childhood brain tumors. Curr. Neurol. Neurosci. Rep. 2001; 1(2):137–143. [PubMed: 11898509]
32. Saadi W, Wang SJ, Lin F, Jeon NL. A parallel-gradient microfluidic chamber for quantitative analysis of breast cancer cell chemotaxis. Biomed. Microdevices. 2006; 8(2):109–118. [PubMed: 16688570]
33. Sahai E. Mechanisms of cancer cell invasion. Curr. Opin. Genet. Dev. 2005; 15(1):87–96. [PubMed: 15661538]
34. Salomon DS, Brandt R, Ciardiello F, Norm-anno N. Epidermal growth factor-related peptides and their receptors in human malignancies. Crit. Rev. Oncol. Hematol. 1995; 19(3):183–232. [PubMed: 7612182]
35. Seroogy KB, Gall CM, Lee DC, Kornblum HI. Proliferative zones of postnatal rat brain express epidermal growth factor receptor mRNA. Brain Res. 1995; 670(1):157–164. [PubMed: 7719717]
36. Shen JY, Chan-Park MB, He B, Zhu AP, Zhu X, Beuerman RW, Yang EB, Chen W, Chan V. Three-dimensional microchannels in biodegradable polymeric films for control orientation and phenotype of vascular smooth muscle cells. Tissue Eng. 2006; 12(8):2229–2240. [PubMed: 16968163]
37. Wechsler-Reya R, Scott MP. The developmental biology of brain tumors. Annu. Rev. Neurosci. 2001; 24:385–428. [PubMed: 11283316]
38. Xia P, Bungay PM, Gibson CC, Kovbasnjuk ON, Spring KR. Diffusion coefficients in the lateral intercellular spaces of Madin-Darby canine kidney cell epithelium determined with caged compounds. Biophys. J. 1998; 74(6):3302–3312. [PubMed: 9635784]
39. Yamada KM, Cukierman E. Modeling tissue morphogenesis and cancer in 3D. Cell. 2007; 130(4): 601–610. [PubMed: 17719539]
40. Yarden Y. The EGFR family and its ligands in human cancer signalling mechanisms and therapeutic opportunities. Eur. J. Cancer. 2001; 37(Suppl 4):S3–S8. [PubMed: 11597398]
41. Yuan L, Santi M, Rushing EJ, Cornelison R, MacDonald TJ. ERK activation of p21 activated kinase-1 (Pak1) is critical for medulloblastoma cell migration. Clin. Exp. Metastasis. 2010; 27(7): 481–491. [PubMed: 20526801]
42. Yuan, K.; Singh, R.; Rezonzew, G.; Siegal, GP. In vitro matrices for studying tumor cell invasion. In: Wells, A., editor. Cell Motility in Cancer Invasion and Metastasis. Vol. Vol. 8. Springer; New York: 2006. p. 25-54.
43. Zohrabian VM, Forzani B, Chau Z, Murali R, Jhanwar-Uniyal M. Rho/ROCK and MAPK signaling pathways are involved in glioblastoma cell migration and proliferation. Anticancer Res. 2009; 29(1):119–123. [PubMed: 19331140]

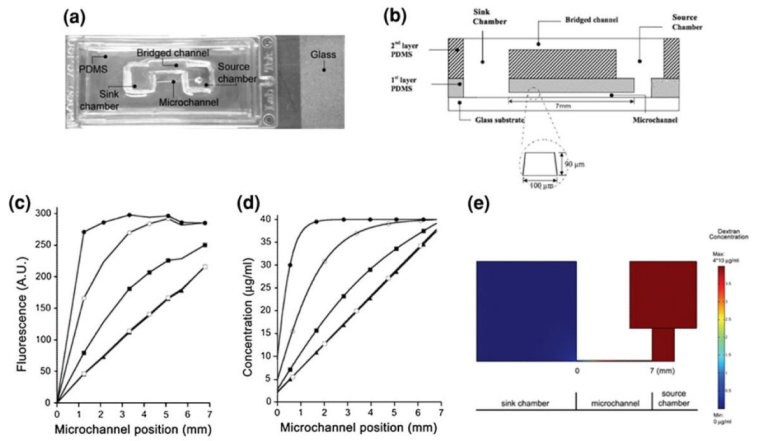

FIGURE 1.

Characterization of the *μ*Lane system for molecular transport. (a) Image and (b) schematics of the *μ*Lane system. (c) Measurement of Dextran concentration profiles within a 7-mm-long microchannel over time. The Dextran fluorescence (arbitrary units) decay with time is plotted against the length of the microchannel (●, $t = 16$ min; □, $t = 3$ h; ■, $t = 14$ h; ○, $t = 70$ h; ▲, $t = 111$ h). The concentration profiles reaches a linear, steady-state at $t = 70$ h. (d) Computational simulation of Dextran concentration profiles formed within the microchannel. Computationally-derived changes in Dextran concentration within the channel over time are plotted against the length of the microchannel (●, $t = 16$ min; □, $t = 3$ h; ■, $t = 14$ h; ○, $t = 70$ h; ▲, $t = 111$ h). (e) Finite Element Modeling of Dextran concentration profiles generated within the microchannel and in the source and sink chambers, respectively.

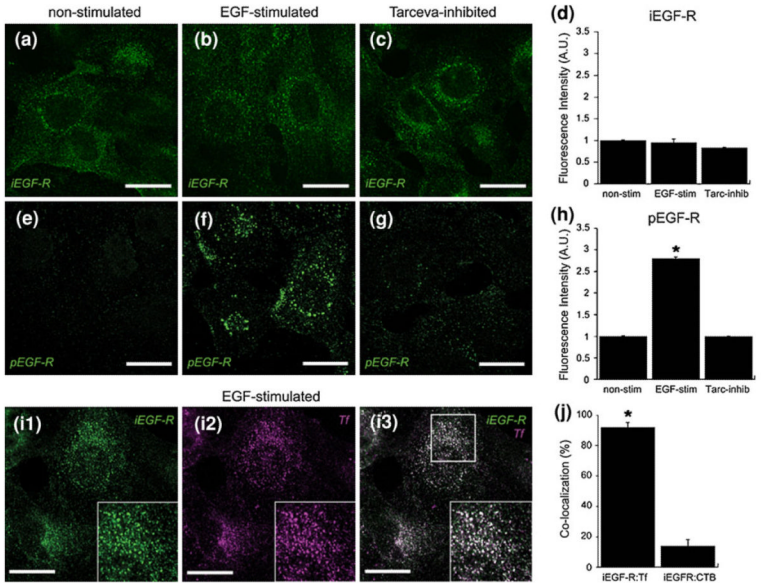

FIGURE 2.

EGF-R phosphorylation levels and localization are mediated by EGF pathway stimulation and inhibition in MB-derived cells. Localization of total EGF-R (iEGF-R) in non-stimulated cells (a), in cells stimulated with 1000 ng/mL EGF (b) and in cells in which EGF signaling was inhibited by 1 μM Tarceva (c). (d) Levels of iEGF-R are not changed due to activation/inactivation of the EGF pathway. Localization of phosphorylated EGF-R (pEGF-R) in non-stimulated cells (e), in cells stimulated with 1000 ng/mL EGF (f) and in cells in which EGF signaling was inhibited by 1 μM Tarceva (g). (h) Levels of pEGF-R are significantly increased due to activation of the EGF pathway. (i) iEGF-R (green) (i1) accumulates in Transferrin (Tf)-positive vesicles (purple) (i2) in EGF-stimulated cells; merged channels (i3). Insert shows higher magnification of the boxed area and co-localization between iEGF-R and Tf. (j) Co-localization between iEGF-R and Tf-positive vesicles, and between iEGF-R and CT-B-positive vesicles in EGF-stimulated cells. Scale bars, 20 μm. * $p < 0.05$.

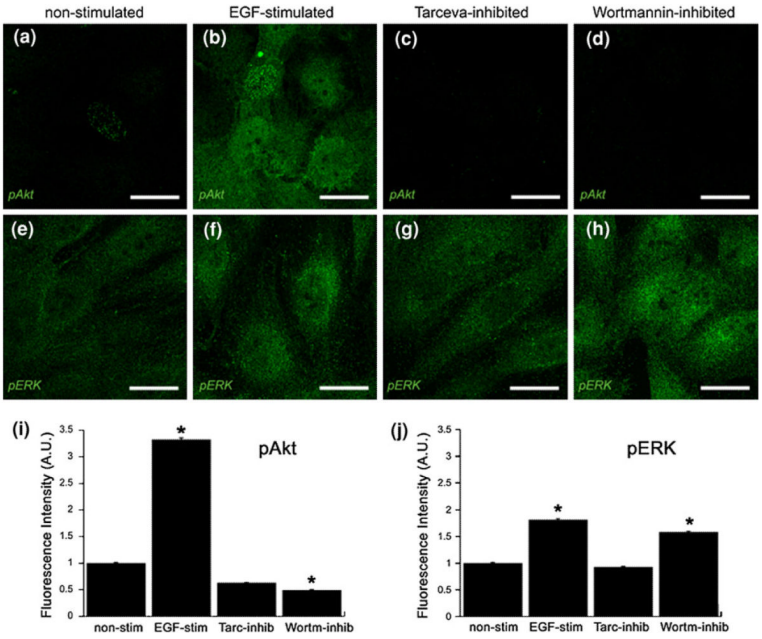

FIGURE 3.

Akt phosphorylation levels and localizations are mediated by EGF pathway stimulation and inhibition in MB-derived cells. Localization of phosphorylated Akt (pAkt) in non-stimulated cells (a), in cells stimulated with 1000 ng/mL EGF (b) cells in which EGF signaling was inhibited by 1 μM Tarceva (c), and cells in which PI3K signaling was inhibited by 0.5 μM Wortmannin (d). Localization of phosphorylated pERK in non-stimulated cells (e), in cells stimulated with 1000 ng/mL EGF (*F*), cells in which EGF signaling was inhibited by 1 μM Tarceva (g), and cells in which PI3K signaling was inhibited by Wortmannin (h). Scale bars, 20 μm. Quantification of pAkt (i) and pERK (j) in non-stimulated cells, cells stimulated with EGF, cells in which EGF signaling was inhibited with Tarceva and cells in which PI3K signaling was inhibited with Wortmannin. * $p < 0.05$.

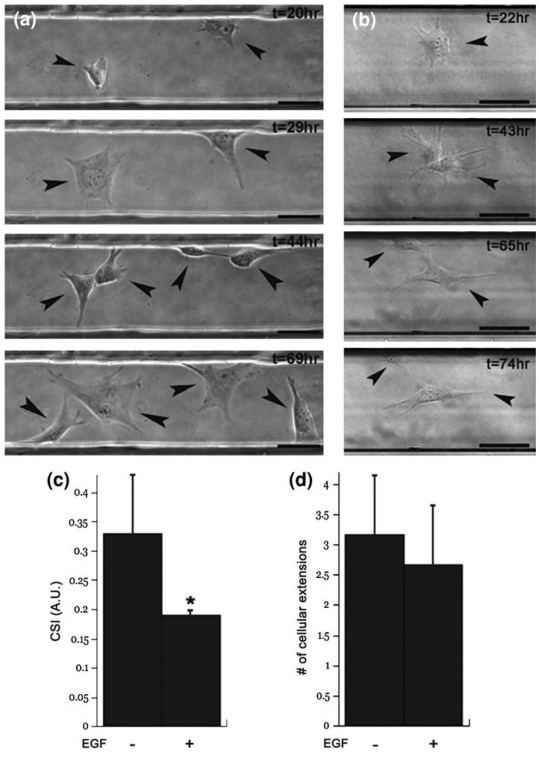

FIGURE 4.

EGF induces morphological changes in MB-derived cells. (a) Cells grow and divide within 3D matrix inside of the microchannel in the absence of EGF. Arrowheads point to the dividing cells and the resulting daughter cells. (b) Cells in the presence of 100 ng/mL EGF within 3D matrix inside of the microchannel. Arrowheads point to the dividing cells and the resulting daughter cells. Scale bars, 50 μm. (c) Cellular Shape Index (CSI) of cells grown within 3D matrix in microchannels in the absence of EGF and in the presence of 100 ng/mL EGF (sample size: $n = 37$, $n_{EGF} = 21$). * $p < 0.05$. (d) Number of cellular extensions in the absence of EGF and in the presence of 100 ng/mL EGF (sample size: $n = 37$, $n_{EGF} = 21$). Scale bars, 50 μm.

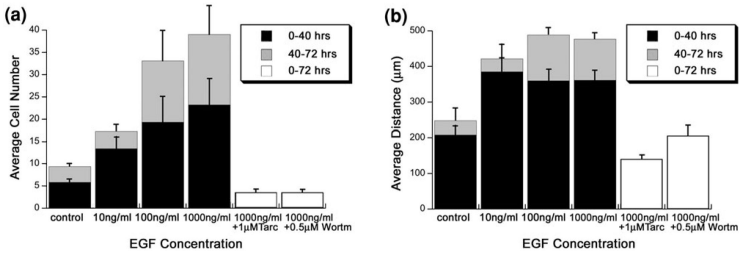

FIGURE 5.

Increasing EGF concentration profiles target the invasion of a large number of MB-derived cells, and this migration is modulated by PI3K. MB-derived cells were exposed to 0, 10, 100, and 1000 ng/mL EGF concentration gradients for 72 h. Additionally, MB-derived cells treated separately with 1 μM EGF-R inhibitor Tarceva, and 0.5 μM PI3K inhibitor Wortmannin were exposed to 1000 ng/ml EGF concentration gradients for 72 h. (a) Number of invading cells is dependent on the activation of EGF downstream pathway. The average numbers of invading cells are represented with standard error bars (sample size: $n_0 = 7$, $n_{10} = 6$, $n_{100} = 5$, $n_{1000} = 8$, $n_{\text{Tarc}} = 5$, $n_{\text{Wort}} = 3$). * $p < 0.05$. (b) Distance invaded by MB-derived cells is dependent on the activation of EGF downstream pathway. The average distances invaded into the microchannel are represented with standard error bars (sample size: $n_0 = 6$, $n_{10} = 6$, $n_{100} = 4$, $n_{1000} = 7$, $n_{\text{Tarc}} = 4$, $n_{\text{Wort}} = 3$). * $p < 0.01$. The number of cells as well as distances migrated are represented for both 0–40 h interval (migration only —black), as well as for the 40–72 h interval (migration and proliferation—grey).